Scaling of geostrophic kinetic energy to the spatial variance of sea surface heights

A. Kaplan

Lamont-Doherty Earth Observatory, Palisades, NY 10964

Short title: SPATIAL VARIANCE OF SEA SURFACE HEIGHTS

Abstract. A quantitative connection is established between two measures of mesoscale variability: the ocean near-surface geostrophic kinetic energy and the small-scale spatial variance of sea surface heights (SSH). The former is traditionally used in diagnostic studies of ocean eddies. The latter is defined as a spatial variance of SSH inside grid boxes of a given size and represents a basic statistical characteristic of the SSH field, necessary for estimating its vulnerability to sampling and gridding error. The connection manifests itself in a striking similarity between patterns of sea surface height error and of eddy kinetic energy. Under the condition of isotropic distribution of mesoscale energy, simple formulas connecting the two variables are obtained for the long wave, random walk, and white noise versions of the ocean power spectrum. These spectral approximations result in quadratic, linear, and constant scalings of small-scale variability with changing gridsize, respectively. In the case of a general wavenumber power spectrum, the quadratic scaling can be used with a correction coefficient depending on the shape but not the magnitude of the power spectrum. Approximations based on one-dimensional power spectrum estimates are developed. They are verified by application to gridded satellite altimetry fields. Spatial non-stationarity of the spectral shape is shown to be necessary for a good fit.

1. Introduction

Oceanographers have long been interested in the global distribution of mesoscale variability in the ocean. With progress in satellite altimetry, techniques for estimating this pattern have been getting more elaborate, and the pattern estimates themselves more detailed. Early estimates of this pattern were based on just a month of SEASAT data (Cheney et al. 1983), or a year of the Geosat mission (Fu et al. 1988), and mesoscale variability was expressed in terms of the temporal standard deviation of altimetric values from repeat tracks. In the Topex/Poseidon (T/P) period an explicit computation of the near-surface geostrophic kinetic energy (GKE) became the most common way to map the mesoscale variability. Stammer (1997) (hereafter S97) used only along-track derivatives of altimetric values, under the assumption of isotropy of the turbulent eddy field. Later, when merging T/P and ERS-1,2 data allowed gridding of global sea surface height (SSH) fields $s(x, y, t)$ with resolution as fine as $\Delta x = \Delta y = 0.25^o$ in space and $\Delta t = 10$ day in time, Ducet et al. (2000) (hereafter DLTR) computed eddy kinetic energy as the GKE $\mathcal{K}$:

$$\mathcal{K} = \mathcal{K}_u + \mathcal{K}_v = \frac{u_g^2}{2} + \frac{v_g^2}{2} = \frac{g^2}{2f^2}\mathcal{G}, \tag{1}$$

where

$$\mathcal{G} = |\vec{\nabla} s|^2 = \mathcal{G}_x + \mathcal{G}_y = \left(\frac{\partial s}{\partial x}\right)^2 + \left(\frac{\partial s}{\partial y}\right)^2$$

is a squared gradient of SSH, g is the acceleration of gravity, and $f = 2\Omega \sin\theta$ is the Coriolis parameter at latitude θ ($\Omega = 2\pi$/day is the earth rotation rate). Unlike $\mathcal{K}$, the field of $\mathcal{G} = (2f^2/g^2)\mathcal{K}$ does not have the equatorial singularity due to the vanishing Coriolis parameter (cf. Figures 1a and 1b), and thus is more convenient for computing and visualizing.

Another measure of mesoscale variability, variance of the SSH inside a space-time box

$L_x \times L_y \times L_t$ is defined as

$$\sigma^2_{L_x \times L_y \times L_t} = [s^2]_{L_x \times L_y \times L_t} - [s]^2_{L_x \times L_y \times L_t},$$

where square brackets denote an average over the domain indicated by a subindex. Interest to such characteristics of geophysical field variability is due to the role they play in evaluation of sampling and gridding error (Trenberth et al. 1992; Kaplan et al. 1997, 2000; Rayner et al. 2003). The pattern of $\langle \sigma^2_{L_x \times L_y \times L_t} \rangle$ (Figure 1c) persistently appears in error estimates of gridded altimetry products and model SSH fields (DLTR; Le Traon and Dibarboure, 2002; Kaplan et al. 2004). (Hereafter angle brackets denote long-term averages interpreted here as "expectations", i.e. as estimates of the statistical ensemble mean). This pattern looks similar to the pattern of the mean squared SSH gradient $\langle \mathcal{G} \rangle$, and resembles the GKE pattern $\langle \mathcal{K} \rangle$ too, due to the connection (1) between the latter two (Figures 1a-c). This similarity results in the patterns of the SSH gridding error and of the GKE looking quite similar (e.g. DLTR Plates 1 and 8), despite they describe different variables.

To explain the similarity between $\langle \sigma^2_{L_x \times L_y \times L_t} \rangle$ and $\langle \mathcal{G} \rangle$, note that the former can be presented as

$$\sigma^2_{L_x \times L_y \times L_t} = [\sigma^2_{L_x \times L_y}]_{L_t} + \tau^2_{L_t},$$

where the first term in the right-hand side is a time-average of spatial small-scale variability (SSV) $\sigma^2_{L_x \times L_y} = [s^2]_{L_x \times L_y} - [s]^2_{L_x \times L_y}$, and the second term represents the short-term variance of the spatial means $\tau^2_{L_t} = [[s]^2_{L_x \times L_y}]_{L_t} - [s]^2_{L_x \times L_y \times L_t}$. Therefore for long-term averages obtain

$$\langle \sigma^2_{L_x \times L_y \times L_t} \rangle = \langle \sigma^2_{L_x \times L_y} \rangle + \langle \tau^2_{L_t} \rangle.$$

For mesoscale variability the first term on the right is the major part of the sum due to the dispersion relation for planetary waves (Kaplan et al. 2004). Accordingly, the patterns of

$\langle \sigma^2_{L_x \times L_y \times L_t} \rangle$ and $\langle \sigma^2_{L_x \times L_y} \rangle$ are quite similar (Figures 1c and 1d). On the other hand, the SSV $\langle \sigma^2_{L_x \times L_y} \rangle$ and mean squared SSH gradient $\langle \mathcal{G} \rangle$ have very similar patterns, because of a mathematical connection which exists between these two.

The purpose of this paper is to derive and verify this connection between $\langle \sigma^2_{L_x \times L_y} \rangle$ and $\langle \mathcal{G} \rangle$ (and thus the GKE $\langle \mathcal{K} \rangle$). Not only does this connection provide a quantitative explanation to the similarity between the GKE and the SSH gridding error fields, but it also gives a simple way to estimate GKE if SSV is known, and vice versa. This connection will allow us to see how $\mathcal{K}$ or $\mathcal{G}$, usually computed for the smallest resolved scales of the SSH field "scale up" to the spatial variability inside boxes of some larger size $L_x \times L_y$.

In Section 2 simple formulas are derived for special cases when the isotropically turbulent ocean is dominated by very long waves (compared to L_x and L_y) or when its SSH fieldis described by white noise or random walk processes. When these simplifying assumptions are not used, the connection between the SSV and GKE involves a coefficient which depends on the shape of the wavenumber power spectrum of the ocean SSH (Section 3). Approximations based on one-dimensional power spectrum estimates are developed. They are verified by application to the DLTR data set of satellite altimetry fields in Section 4. Discussion and conclusions are presented in Section 5.

2. Special cases for the isotropic ocean

The isotropy assumption for the GKE is equivalent to the statement that the expected square of the SSH partial derivative does not depend on the direction of differentiation $\vec{n}$:

$$\left\langle \left(\frac{\partial s}{\partial \vec{n}} \right)^2 \right\rangle = \langle \mathcal{G}_x \rangle = \langle \mathcal{G}_y \rangle = \langle \mathcal{G} \rangle / 2. \tag{2}$$

Long-wave approximation. Suppose SSH values $s(x,y,t)$ are available on a fine grid with steps $\Delta x = L_x/M$ and $\Delta y = L_y/N$ inside a gridbox $L_x \times L_y$ of a sparser grid. If the SSH field is dominated by the waves longer than L_x and L_y, then for any two gridpoints (m_1,n_1) and (m_2,n_2) inside the $L_x \times L_y$ box the assumption (2) results in the following expression for the expected value

$$\left\langle \left(\frac{s_{m_1,n_1} - s_{m_2,n_2}}{\sqrt{(m_1-m_2)^2\Delta x^2 + (n_1-n_2)^2\Delta y^2}} \right)^2 \right\rangle = \frac{1}{2}\langle \mathcal{G} \rangle.$$

It is easy to check that for a sample comprised of all gridded values $s_{m,n}$ inside a spatial gridbox $L_x \times L_y$, the SSV can be written as

$$\hat{\sigma}^2_{L_x \times L_y} = \frac{1}{2}\left[(s_{m_1,n_1} - s_{m_2,n_2})^2 \right]_{(m_1,n_1)\neq(m_2,n_2)}. \tag{3}$$

(Hereafter hat signifies unbiased sample estimates). Therefore

$$\begin{aligned} \langle \hat{\sigma}^2_{L_x \times L_y} \rangle &= \frac{1}{2}\langle \left[(s_{m_1,n_1} - s_{m_2,n_2})^2 \right]_{(m_1,n_1)\neq(m_2,n_2)} \rangle = \\ &= \frac{1}{4}\langle \mathcal{G} \rangle \left(\left[(m_1-m_2)^2 \right]_{m_1 \neq m_2} \Delta x^2 + \left[(n_1-n_2)^2 \right]_{n_1 \neq n_2} \Delta y^2 \right) = \\ &= \frac{1}{24}\langle \mathcal{G} \rangle \left(M(M+1)\Delta x^2 + N(N+1)\Delta y^2 \right) \approx \frac{L_x^2 + L_y^2}{24}\langle \mathcal{G} \rangle, \end{aligned} \tag{4}$$

where Δx and Δy were neglected in comparison with L_x and L_y respectively ($M \gg 1,\ N \gg 1$).

Random walk approximation. In this case

$$\langle (s_{m+1,n} - s_{m,n})^2 \rangle = \frac{1}{2}\langle \mathcal{G} \rangle \Delta x^2, \qquad \langle (s_{m,n+1} - s_{m,n})^2 \rangle = \frac{1}{2}\langle \mathcal{G} \rangle \Delta y^2$$

holds, but the differences between neighboring points are uncorrelated with each other. Thus

$$\langle (s_{m_1,n_1} - s_{m_2,n_2})^2 \rangle = \frac{1}{2}\langle \mathcal{G} \rangle (|m_1 - m_2|\Delta x^2 + |n_1 - n_2|\Delta y^2)$$

(variance grows as in a typical random walk process). Using (3) and making the same approximation as in (4), obtain

$$\langle \hat{\sigma}^2_{L_x \times L_y} \rangle = \frac{1}{12}\langle \mathcal{G} \rangle [(M+1)\Delta x^2 + (N+1)\Delta y^2] \approx \frac{L_x \Delta x + L_y \Delta y}{12}\langle \mathcal{G} \rangle. \tag{5}$$

White noise. If values of s at different grid points are not correlated with each other, then $\langle\hat{\sigma}^2_{L_x\times L_y}\rangle$ does not depend at all on L_x or L_y:

$$\langle\hat{\sigma}^2_{L_x\times L_y}\rangle = \frac{1}{\Delta x^{-2}+\Delta y^{-2}}\langle\mathcal{G}\rangle. \tag{6}$$

General relationship. Define

$$\alpha_{L_x\times L_y} = \frac{12}{L_x^2+L_y^2}\frac{\langle\hat{\sigma}^2_{L_x\times L_y}\rangle}{\langle\mathcal{G}\rangle}. \tag{7}$$

Formulas (4), (5), and (6) can be written then as

$$\langle\hat{\sigma}^2_{L_x\times L_y}\rangle = \alpha_{L_x\times L_y}\frac{L_x^2+L_y^2}{12}\langle\mathcal{G}\rangle. \tag{8}$$

Here $\alpha_{L_x\times L_y}\approx$0.5 in the long-wave case (cf. (4)), while in the two other cases (random walk and white noise) $\alpha_{L_x\times L_y}\ll 1$ if $\Delta x\ll L_x$ and $\Delta y\ll L_y$ (cf. (5), (6)). This suggests that for the isotropically turbulent ocean, formula (4) gives an upper-bound for the ratio $\alpha_{L_x\times L_y}$. The value of $\alpha_{L_x\times L_y}$ reaches 0.5 for the isotropic ocean dominated by waves much longer than L_x and L_y, but tends to zero when decorrelation scales of the SSH field become small compared to the box dimensions.

3. Ocean with a general power spectrum

Individual waves. Suppose a waveform of a unit amplitude with wavenumbers k_x and k_y

$$s(x,y,t) = \Re\, e^{i2\pi(k_x x+k_y y-\omega t+\varphi_o)}$$

propagates through a space box of dimensions L_x and L_y (φ_o is an arbitrary phase shift). It is easy to calculate that, averaged over all phases φ_o,

$$\sigma^2_{L_x\times L_y} = 1-\mathcal{C}(\lambda_x)\mathcal{C}(\lambda_y), \tag{9}$$

where $\lambda_x = k_x L_x$ and $\lambda_y = k_y L_y$ are dimensionless parameters and

$$\mathcal{C}(\lambda) = \left(\frac{\sin \pi\lambda}{\pi\lambda}\right)^2$$

(Kaplan et al., 2004, Sec. A1). Note that $\mathcal{C}(0) = 1$ and $0 \le \mathcal{C}(\lambda) \le 1$ for all λ, since $|\sin x/x| \le 1$. If spatial averaging is done only in x (or y) direction, obtain from (9) formulas for one-dimensional variance:

$$\sigma^2_{L_x} = 1 - \mathcal{C}(\lambda_x), \qquad \sigma^2_{L_y} = 1 - \mathcal{C}(\lambda_y). \tag{10}$$

Obviously

$$0 \le \sigma^2_{L_x} \le 1, \qquad 0 \le \sigma^2_{L_y} \le 1$$

and

$$\sigma^2_{L_x \times L_y} = \sigma^2_{L_x} + \sigma^2_{L_y} - \sigma^2_{L_x}\sigma^2_{L_y}. \tag{11}$$

For a single waveform

$$\mathcal{G} = \mathcal{G}_x + \mathcal{G}_y = 4\pi^2(k_x^2 + k_y^2), \tag{12}$$

thus its parameter α is

$$\alpha_{L_x \times L_y}(k_x, k_y) = \frac{12\sigma^2_{L_x \times L_y}}{(L_x^2 + L_y^2)\mathcal{G}} = \varrho(\lambda_x, \lambda_y)\frac{1 + \ell\kappa}{2}, \tag{13}$$

where

$$\varrho(\lambda_x, \lambda_y) = \frac{3(1 - \mathcal{C}(\lambda_x)\mathcal{C}(\lambda_y))}{\pi^2(\lambda_x^2 + \lambda_y^2)}, \tag{14}$$

while ℓ and κ measure the "anisotropy" of the gridbox and of the waveform respectively:

$$\ell = \frac{L_x^2 - L_y^2}{L_x^2 + L_y^2}, \qquad \kappa = \frac{k_x^2 - k_y^2}{k_x^2 + k_y^2}. \tag{15}$$

Both ℓ and κ take values from -1 to 1, reaching these extremes when either of their arguments is 0, and vanishing when the arguments are equal. Therefore, the factor

$(1+\ell\kappa)/2$ in (13) is close to 1/2 if either ℓ or κ is small, but can reach 1 (or 0), if they approach their extremes of the same (or opposite) sign. The function $\varrho(\lambda_x,\lambda_y)\to 0$ when $\lambda_x^2+\lambda_y^2\to\infty$. When $\lambda_x^2+\lambda_y^2\to 0$, $\varrho\to 1$, since for small λ_x and λ_y the approximation $\mathcal{C}(\lambda)=1-\pi^2\lambda^2/3+o(\lambda^3)$ can be used, and (14) gives

$$\varrho(\lambda_x,\lambda_y)\approx\frac{3\pi^2(\lambda_x^2+\lambda_y^2)/3}{\pi^2(\lambda_x^2+\lambda_y^2)}=1.$$

Therefore $0\le\alpha_{L_x\times L_y}(k_x,k_y)\le 1$. In the long-wave limit ($\lambda_x\ll 1,\ \lambda_y\ll 1$), for the waveforms with $\kappa\approx 0$ formula (13) gives $\alpha=1/2$, in agreement with (4).

It is easy to check that the formula (13) for α works for one-dimensional averages as well, if both the wavenumber and gridsize of an "unused" dimension are put to zero (resulting in $\ell\kappa=1$):

$$\begin{aligned}\alpha_{L_x}(k_x) &= \frac{12}{L_x^2}\frac{\sigma_{L_x}^2}{\mathcal{G}_x}=\frac{3(1-\mathcal{C}(\lambda_x))}{\pi^2k_x^2L_x^2}=\alpha_{L_x\times 0}(k_x,0),\\ \alpha_{L_y}(k_y) &= \frac{12}{L_y^2}\frac{\sigma_{L_y}^2}{\mathcal{G}_y}=\frac{3(1-\mathcal{C}(\lambda_y))}{\pi^2k_y^2L_y^2}=\alpha_{0\times L_y}(0,k_y).\end{aligned}\tag{16}$$

Spectral distribution. Let

$$s(x,y)=\int_{-\infty}^{\infty}\int_{-\infty}^{\infty}\xi(k_x,k_y)e^{2\pi i(k_xx+k_yy}dk_xdk_y.$$

Assume $\xi(-k_x,-k_y)=\xi(k_x,k_y)^*$ to guarantee that s is real (an asterisk denotes complex conjugation). Also assume that amplitudes of waves with different wavenumbers are statistically independent:

$$\langle\xi(k_k,k_y)\xi(l_x,l_y)^*\rangle=\mathcal{P}(k_x,k_y)\delta(k_x-l_x)\delta(k_y-l_y),$$

where $\mathcal{P}(k_x,k_y)$ is the two-dimensional wavenumber power spectrum of s. It is easy to show that for the ocean with a known SSH wavenumber spectrum $\mathcal{P}(k_x,k_y)$ the ratio $\alpha^{\mathcal{P}}_{L_x\times L_y}$ can

be computed as

$$\alpha^{\mathcal{P}}_{L_x\times L_y} = \frac{12}{L_x^2+L_y^2}\frac{\int_{-\infty}^{\infty}\int_{-\infty}^{\infty}\sigma^2_{L_x\times L_y}\mathcal{P}dk_xdk_y}{\int_{-\infty}^{\infty}\int_{-\infty}^{\infty}\mathcal{G}\mathcal{P}dk_xdk_y} = \frac{\int_{-\infty}^{\infty}\int_{-\infty}^{\infty}\alpha_{L_x\times L_y}(k_x,k_y)\mathcal{G}\mathcal{P}dk_xdk_y}{\int_{-\infty}^{\infty}\int_{-\infty}^{\infty}\mathcal{G}\mathcal{P}dk_xdk_y}. \tag{17}$$

Note that since $\mathcal{G}\mathcal{P}$ is positive, by the mean value theorem (e.g. Buck, 1965)

$$\alpha^{\mathcal{P}}_{L_x\times L_y} = \alpha_{L_x\times L_y}(k_x', k_y'),$$

for certain k_x' and k_y'. Therefore $\alpha^{\mathcal{P}}_{L_x\times L_y}$ has to lie between 0 and 1 as well.

One-dimensional averages for discrete fields. In practical computations for the data gridded with steps Δx and Δy equations (10) and (12) become

$$\hat{\sigma}^2_{L_x} = \frac{M}{M-1}\left(1-\frac{\sin^2\pi k_xL_x}{M^2\sin^2\pi k_x\Delta x}\right), \quad \hat{\sigma}^2_{L_y} = \frac{N}{N-1}\left(1-\frac{\sin^2\pi k_yL_y}{N^2\sin^2\pi k_y\Delta y}\right),$$

$$\hat{\mathcal{G}} = \hat{\mathcal{G}}_x + \hat{\mathcal{G}}_y = (\Delta x)^{-2}\sin^2 2\pi k_x\Delta x + (\Delta y)^{-2}\sin^2 2\pi k_y\Delta y.$$

Therefore the coefficients for one-dimensional averages can be computed as

$$\hat{\alpha}^{\mathcal{P}}_{L_x} = \frac{12}{L_x^2}\frac{\int_{-\infty}^{\infty}\hat{\sigma}^2_{L_x}\mathcal{P}_x(k_x)dk_x}{\int_{-\infty}^{\infty}\hat{\mathcal{G}}_x\mathcal{P}_x(k_x)dk_x}, \qquad \hat{\alpha}^{\mathcal{P}}_{L_y} = \frac{12}{L_y^2}\frac{\int_{-\infty}^{\infty}\hat{\sigma}^2_{L_y}\mathcal{P}_y(k_y)dk_y}{\int_{-\infty}^{\infty}\hat{\mathcal{G}}_y\mathcal{P}_y(k_y)dk_y}, \tag{18}$$

where

$$\mathcal{P}_x(k_x) \propto \int_{-\infty}^{\infty}\mathcal{P}(k_x,k_y)dk_y, \qquad \mathcal{P}_y(k_y) \propto \int_{-\infty}^{\infty}\mathcal{P}(k_x,k_y)dk_x$$

are one-dimensional wavenumber spectra in zonal and meridional directions.

Estimates for two-dimensional averages. Multiply both sides of (11) by $\mathcal{P}$ and integrate over k_x and k_y. By (10) and the mean value theorem, for a certain k_x'

$$\sigma^{2\,\mathcal{P}}_{L_x\times L_y} = \sigma^{2\,\mathcal{P}}_{L_x} + \int_{-\infty}^{\infty}\int_{-\infty}^{\infty}(1-\sigma^2_{L_x})\sigma^2_{L_y}\mathcal{P}dk_xdk_y = \sigma^{2\,\mathcal{P}}_{L_x} + \mathcal{C}(k_x'L_x)\sigma^{2\,\mathcal{P}}_{L_y}, \tag{19}$$

where $\sigma^{2\,\mathcal{P}}$ denotes the SSV for the ocean with the power spectrum $\mathcal{P}$ Dividing by $\langle\mathcal{G}\rangle(L_x^2+L_y^2)/12$, obtain

$$\alpha^{\mathcal{P}}_{L_x\times L_y} = a_x + \mathcal{C}(k_x'L_x)a_y,$$

where

$$a_x = \frac{1}{4}\left[(1+\gamma)(1+\ell)\alpha^{\mathcal{P}}_{L_x}\right], \qquad a_y = \frac{1}{4}\left[(1-\gamma)(1-\ell)\alpha^{\mathcal{P}}_{L_y}\right].$$

Here $\gamma = (\mathcal{G}_x - \mathcal{G}_y)/(\mathcal{G}_x + \mathcal{G}_y)$ measures local anisotropy of variations in the SSH and ℓ is the "anisotropy" in the grid, introduced by (15). Since a similar equation can be written for x and y switched, one can write

$$\alpha^{\mathcal{P}}_{L_x \times L_y} = \max(a_x, a_y) + \mathcal{C}(\lambda'_{\max}) \min(a_x, a_y). \tag{20}$$

With the values of $\mathcal{C}$ being between 0 and 1, equation (20) provides both upper and lower bounds for $\alpha^{\mathcal{P}}_{L_x \times L_y}$.

4. Verification

"Observational" values of α can be computed from the gridded analyses of satellite altimetry by DLTR using (7). Long-term averaging is done over October 22, 1992 – Aug 6, 2001, with the exception of a data gap from December 24, 1993 to March 24, 1995.

One-dimensional averages. Observational ratios α_{L_x} and α_{L_y} for $L_x = L_y = 4^o$ are shown in Figures 2a and 2b. They manifest a discernible latitudinal dependence (particularly for α_{L_y}), which underlies more localized features. The dependence on the latitude becomes even more obvious in their zonal means presented in Figure 3 (thick lines) for L_x and L_y taking values 2^o, 4^o, and 8^o. Nonphysical values of α which exceed 1 due to severe undersampling are excluded from spatial averaging hereafter.

Theoretical values and spectral approximation. To compute theoretical values of α, the SSH wavenumber spectrum $\mathcal{P}$ is needed. If $\mathcal{P}$ is approximated as $\mathcal{P} = A(x,y)B(k_x,k_y)$, where A is the total local spectral energy, and B is a globally-universal normalized spectral shape, the coefficients α computed by (17) or (18) will not depend on the amplitude A,

and thus will not depend on x or y (aside from the dependence on y due to the latitudinal variation in the length of L_x, if L_x is fixed in degrees of longitude). In other words, stationary approximations of the wavenumber spectrum, which assume independence of the spectral shape B from x and y (e.g., DLTR) will result in near-constant spatial fields of α. Therefore the dependence of spectral slopes and transition points on the location, especially on latitude (S97), is necessary for obtaining realistic spatial distributions of α (Figures 2 and 3).

The form of the non-stationary along-track power spectrum found by S97 involves $k^{-2.5}$ relationship in the tropical oceans and consists of three distinct spectral fragments with exponents -0.7, -2.8, and -4.6 in midlatitudes, the transition points being defined in terms of normalized wavenumbers. Here these two spectral forms are joint into a single spectral curve:

$$\Gamma(\tilde{k}) = \begin{cases} \tilde{k}^{-0.7}, & a_- \le \tilde{k} \le b_- \\ b_-^{-0.7-r}\tilde{k}^r, & b_- \le \tilde{k} \le b_+ \\ b_-^{-0.7-r} b_+^{r+4.6}\tilde{k}^{-4.6}, & b_+ \le \tilde{k} \le a_+ \end{cases} \tag{21}$$

where $b_- = \max(a_-, 1.006)$, $a_+ = 4.54$, and $\tilde{k} = k/k_0$ is normalized by the wavenumber of maximum kinetic energy k_0. The latter is presented by S97 as a function of the first-mode baroclinic Rossby radius of deformation L_{Ro} and latitude θ:

$$k_0 = (2\pi(0.8 + \theta/25^o)L_{Ro})^{-1}. \tag{22}$$

Estimates of L_{Ro} by Chelton et al. (1998) were used in (22) to obtain k_0. Location-dependent nature of L_{Ro} and k_0 makes Γ and α location-dependent too.

Poleward of a certain latitude θ_0 parameters in (21) take values determined by S97 for off-tropical spectra: $a_- = 0.18, \quad b_+ = 2.057, \quad r = -2.8$. Equatorward of θ_0, they are interpolated toward their equatorial values (which correspond to a single spectral segment

between $a_-^e k_0$ and $a_+ k_0$) by the formulas

$$a_- = 0.18(1-d) + a_-^e d, \quad b_+ = 2.057(1-d) + 4.54d, \quad r = -2.8(1-d) - 2.5d.$$

In order to get a better fit to the observed values, the interpolation coefficient d is chosen to depend on the latitude θ as $d = (\theta_0 - \theta)^2/\theta_0^2$, the lower limit for normalized equatorial wavenumbers is taken a_-^e=1.5.

One-dimensional power spectra for use in (18) are assumed $\mathcal{P}_x(k_x) = \Gamma(k_x/k_0)$ and $\mathcal{P}_y(k_y) = \Gamma(k_y/k_0)$. The "switching" latitude for the equatorial approximation is taken $\theta_0 = 30^o$ for $\mathcal{P}_x$ and $\theta_0 = 10^o$ for $\mathcal{P}_y$. Integrations are done numerically in the interval of wavenumbers between $a_- k_0$ and $a_+ k_0$. Results show a reasonable agreement with observations (Figure 2), especially for zonal means (Figure 3).

Two-dimensional averages. Figure 4 compares global means of observational and theoretical values of $\alpha_{L_x \times L_y}$ for various combinations of L_x and L_y. Theoretical estimates for $\alpha_{L_x \times L_y}$ are based on the approximation (20). Upper and lower bounds correspond to the values of $\mathcal{C}(\lambda'_{\max})$ taken equal 1 and 0 respectively ($\lambda'_{\max} = 0$ or ∞). Despite imperfections of theoretical values for α_{L_x} and α_{L_y} (Figures 2 and 3), all based on them intervals for $\alpha_{L_x \times L_y}$ indeed contain observational values (Figure 4).

To obtain estimates of $\alpha_{L_x \times L_y}$ value within these intervals, note that the presence of $\mathcal{P}$ in the integral of equation (19) favors the low-wavenumber part of the power spectrum. Therefore $\lambda'_{\max}$ is taken at the midpoint of the flattest (with the exponent -0.7) portion of the spectrum Γ: $\lambda'_{\max} = \tilde{k}' k_0 L_{\max}$ with $\tilde{k}' = (a_- + b_-)/2$. Near the equator this expression gives the smallest wavenumber in which Γ is defined by (21). Figure 4 demonstrates that this approximation has a reasonable skill.

5. Discussion and Conclusions

An explicit connection is established between basic statistical and dynamical characteristics of the SSH field: its SSV $\langle \sigma^2_{L_x \times L\ _y} \rangle$ in a box of dimensions $L_x \times L_y$ and its GKE $\langle \mathcal{K} \rangle$ are related by

$$\langle \sigma^2_{L_x \times L_y} \rangle = \alpha_{L_x \times L_y} \frac{2f^2}{g^2} \frac{L_x^2 + L_y^2}{12} \langle \mathcal{K} \rangle$$

(this combines (8) with (1)). The coefficient $\alpha_{L_x \times L_y}$ is always between 0 and 1 and depends on the shape of wavenumber power spectrum of the SSH and dimensions L_x and L_y. The value of $\alpha_{L_x \times L_y}$ describes how well local SSH differences that determine GKE values scale up to the size of the $L_x \times L_y$ box. Therefore $\alpha_{L_x \times L_y}$ may serve as a useful diagnostic value in various oceanographic analyses. Geographical variations in α which we were able to observe (Figures 2 and 3) imply non-stationarity of the shape of the SSH wavenumber power spectrum. However, changes in α from place to place are limited, thus the visual similarity of Figures 1b and 1d ensues.

If the energy distribution over wave directions and the gridbox geometry are fixed, $\alpha_{L_x \times L_y}$ increases with the wavelength. It tends to zero when waves are very short compared to the grid dimensions and reaches its maximum when the waves are very long. Thus the areas where waves are unusually long have higher values of α. Therefore there is a general increase of α in the equatorial area (Figures 2 and 3) where long equatorial Kelvin and Rossby waves propagate. Also most of the counter current areas and other places with high shear and instability waves are associated with local maxima of α (Figure 2).

The increase in the size of $L_x \times L_y$ grid box causes a decrease in $\alpha_{L_x \times L_y}$. This is clearly confirmed by observations (Figures 3 and 4).

The maximum value that $\alpha_{L_x \times L_y}$ can reach is controlled by the gridbox geometry

in relation to the directional distribution of wave energy. If the distribution is isotropic ($\kappa \ll 1$) or the gridbox is square ($\ell = 0$), the maximum value of α is 0.5. In the case of completely anisotropic and perfectly aligned wave and grid geometry $\kappa\ell = 1$, so the maximum is 1 (in practice this corresponds to one-dimensional averaging, when one of the grid dimensions is set to 0).

In the real ocean α never reaches its theoretical maximum value, since this would require having only infinitely long waves present. Moreover, the good agreement between the observational and theoretical values obtained here (Figures 2-4) does not prove that these values of α are realistic. This agreement only confirms the validity of the formalism developed here and an internal consistency between the DLTR fields and S97 spectra, largely derived from the same data (T/P altimetry) which do not represent ocean waves shorter than 100-200km (DLTR; Le Traon and Dibarboure, 2002). Presence of shorter waves in the real ocean implies values for α which are lower than those in Figures 2-4.

Good agreement between observational and theoretical values helps explain the difference in the latitudinal behavior of α_{L_x} and α_{L_y}. Reduction in the Rossby radius with latitude shifts the power spectra toward shorter waves, which correspond to smaller α ratios. This causes a considerable reduction of α_{L_y} with latitude. In α_{L_x}, on the other hand, the decrease of the Rossby radius with latitude is counterbalanced by the reduction in the length of L_x, in direct proportion to $\cos\theta$. This results in a much weaker dependence of α_{L_x} on latitude.

Excessively uniform zonal structure is brought into the theoretical estimates of α by the uniform zonal structure of the Rossby radius L_{Ro} on which k_0 depends (see (22)). Observed zonal variations of α are due to the deviations of the real ocean power spectrum from its simplified description (21). Detailed interpretation and better estimates of α will

be possible when more detailed estimates of the SSH wavenumber power spectrum are developed in the future.

Acknowledgments. The author is grateful to Drs. Mark Cane and Pierre-Yves Le Traon for their advice on the content and disposition of the manuscript. This research was supported by the NOAA through grants NA06GP0567, NA03OAR4320179, and NA03NES4400012. The hospitality of the Institute for Mathematics and its Applications in University of Minnesota is gratefully acknowledged. This is a Lamont–Doherty Earth Observatory contribution number xxxx.

References

Buck, R.C., 1978: *Advanced Calculus*, 3d ed. McGraw-Hill, New York. 622pp.

Chelton, D. B., R. A. deSzoeke, M. G. Schlax, K. El Naggar and N. Siwertz, 1998: Geographical variability of the first-baroclinic Rossby radius of deformation, *J. Phys. Oceanogr.,* **28**, 433-460.

Cheney, R.E., J.G.Marsh, and B.D. Beckley, 1983: Global mesoscale variability from collinear tracks of Seasat altimetry data. *J. Geophys. Res.*, **88**, 4343-4354.

Ducet, N., P.-Y. Le Traon, and G. Reverdin, 2000: Global high-resolution mapping of ocean circulation from TOPEX/Poseidon and ERS-1 and -2. *J. Geophys. Res.*, **105**, 19,477-19,498.

Fu, L.-L., D.B.Chelton, and V.Zlotnicki, 1988: Satellite altimetry: observing ocean variability from space. *Oceanography*, **1**(2), 4-11 and 58.

Kaplan, A., Y. Kushnir, M. Cane, and M. Blumenthal, 1997: Reduced space optimal analysis for historical data sets: 136 years of Atlantic sea surface temperatures, *J. Geophys. Res.*, **102**, 27835–27860.

Kaplan A., Y. Kushnir, M.A. Cane, 2000: Reduced space optimal interpolation of historical marine sea level pressure: 1854-1992, *J. Climate*, **13**, 2987-3002.

Kaplan, A., M.A. Cane, D. Chen, D.L. Witter, and R.E. Cheney, 2004: Small-scale variability and model error in tropical Pacific sea level, *J. Geophys. Res.*, **109**, C02001, doi:10.1029/2002JC001743.

Le Traon, P.Y. and G. Dibarboure, 2002: Velocity mapping capabilities of present and future altimetry missions: The role of high-frequency signals, *J. Atmos. Ocean Tech*, **19**, 2077-2087.

Rayner, N.A., D.E. Parker, E.B. Horton, C.K. Folland, L.V. Alexander, D.P. Rowell, E.C. Kent, and A. Kaplan, 2003: Global analyses of sea surface temperature, sea ice, and night marine air temperature since the late nineteenth century *J. Geophys. Res.*, **108**(14), 10.1029/2002JD002670.

Stammer D., 1997: Global characteristics of ocean variability estimated from regional TOPEX/Poseidon altimeter measurements, *J. Phys. Oceanogr.,* **27**, 1743-1769.

Trenberth, K.E., J.R. Christy, J.W. Hurrell, 1992: Monitoring Global Monthly Mean Surface Temperatures. *J. Climate*, **5**, 1405–1423.

List of Figures

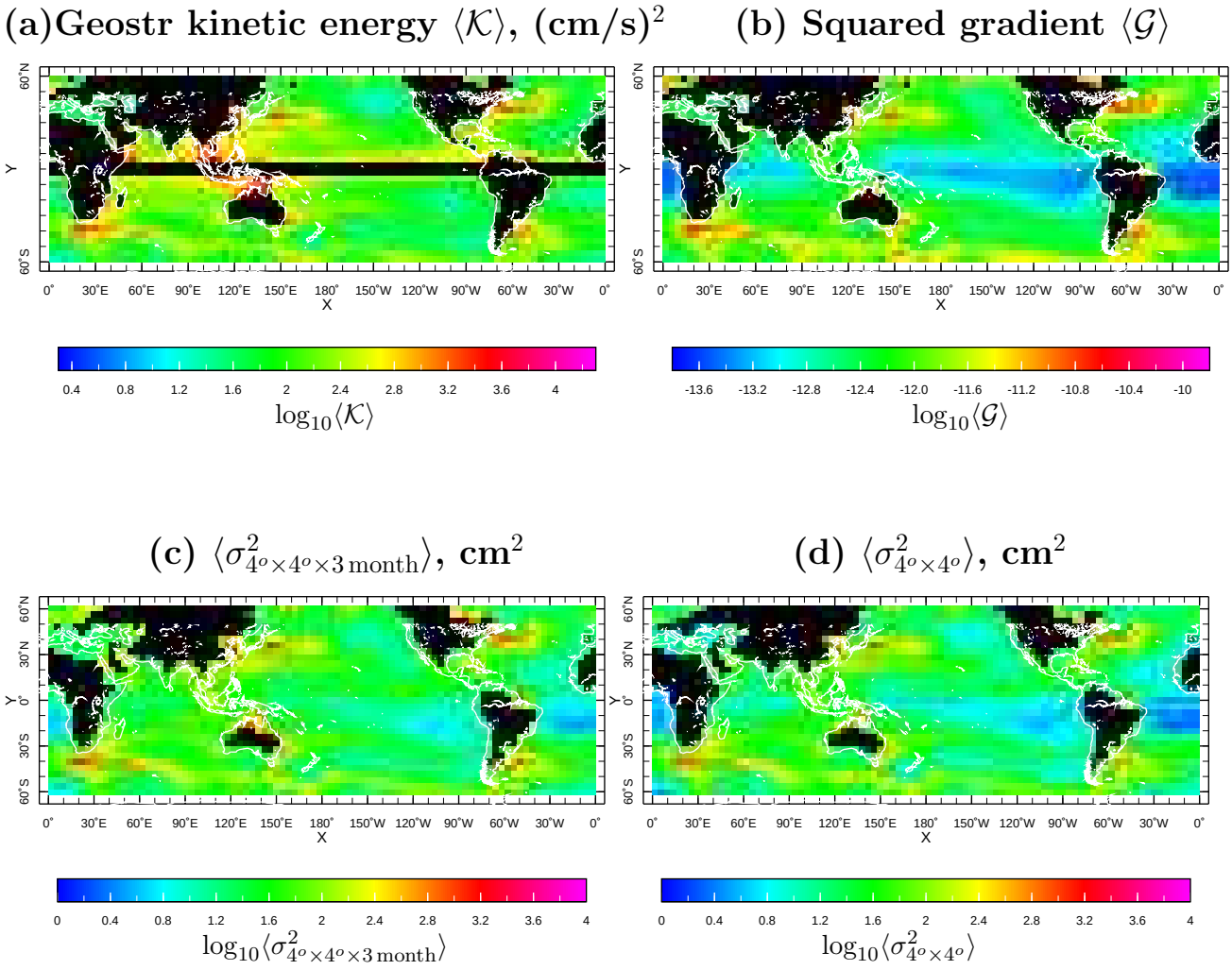

Figure 1. Similarity between SSV and GKE patterns. Shown are base 10 logarithms of numerical values in indicated units of (a) the GKE pattern $\langle \mathcal{K} \rangle$, $(\mathrm{cm/s})^2$, (b) the squared gradient $\langle \mathcal{G} \rangle$, dimensionless, (c) the SSV pattern $\langle \sigma^2_{4^o \times 4^o \times 3\,\mathrm{month}} \rangle$, cm^2 and (d) the SSV pattern $\langle \sigma^2_{4^o \times 4^o} \rangle$, cm^2. Calculations were done using the DLTR satellite altimetry data set for 1992-2001.

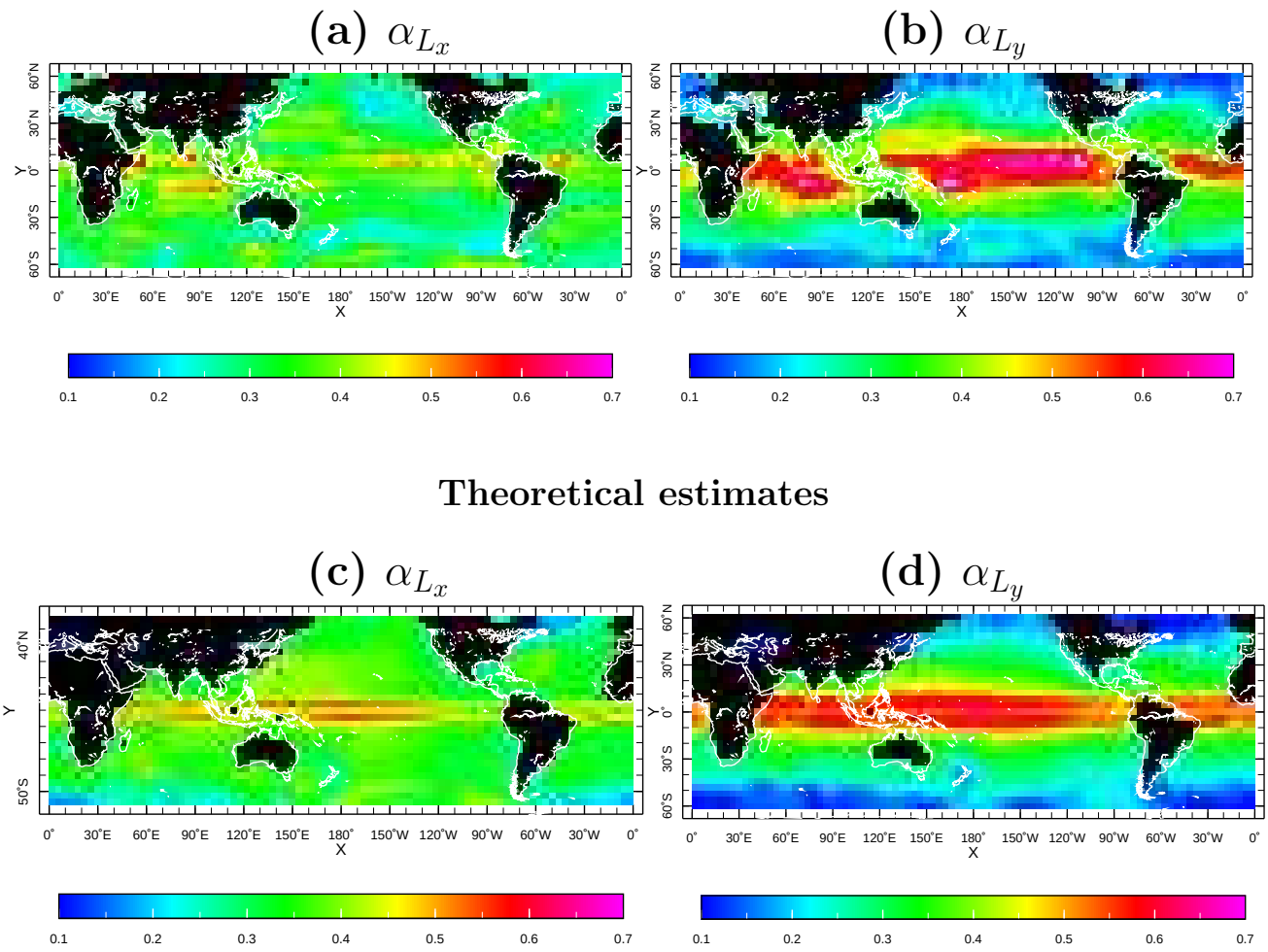

Figure 2. Coefficients α_{L_x} and α_{L_y} for $L_x = L_y = 4^o$ ((a) and (b)) computed from the DLTR data set; estimated theoretically by formula (18) ((c) and (d)).

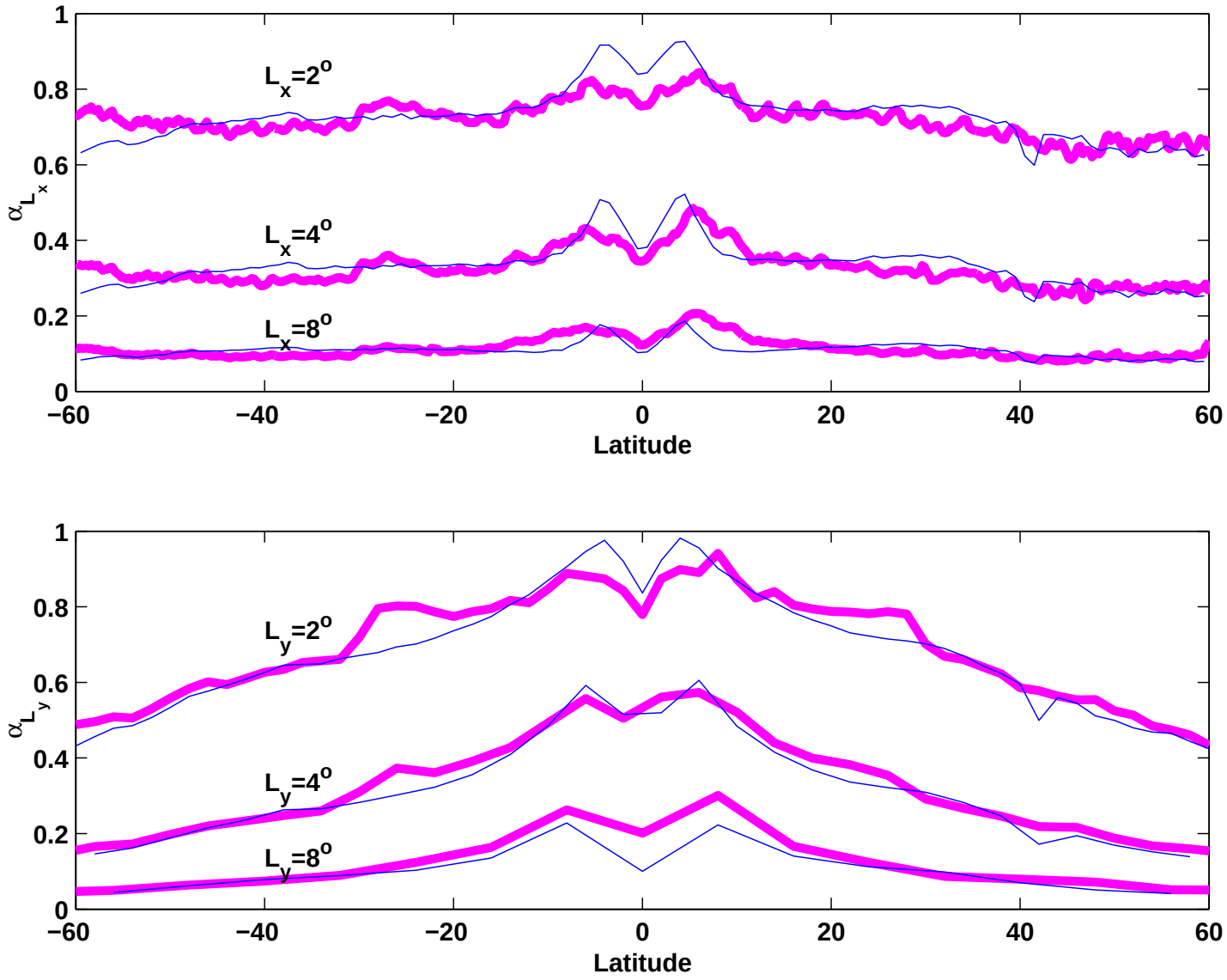

Figure 3. Zonal averages of α_{L_x} (top) and α_{L_y} (bottom) for L_x and L_y equal to 2^o, 4^o, and 8^o. Shown are observational estimates (thick lines) computed from the DLTR data set and theoretical estimates (thin lines) calculated by (18).

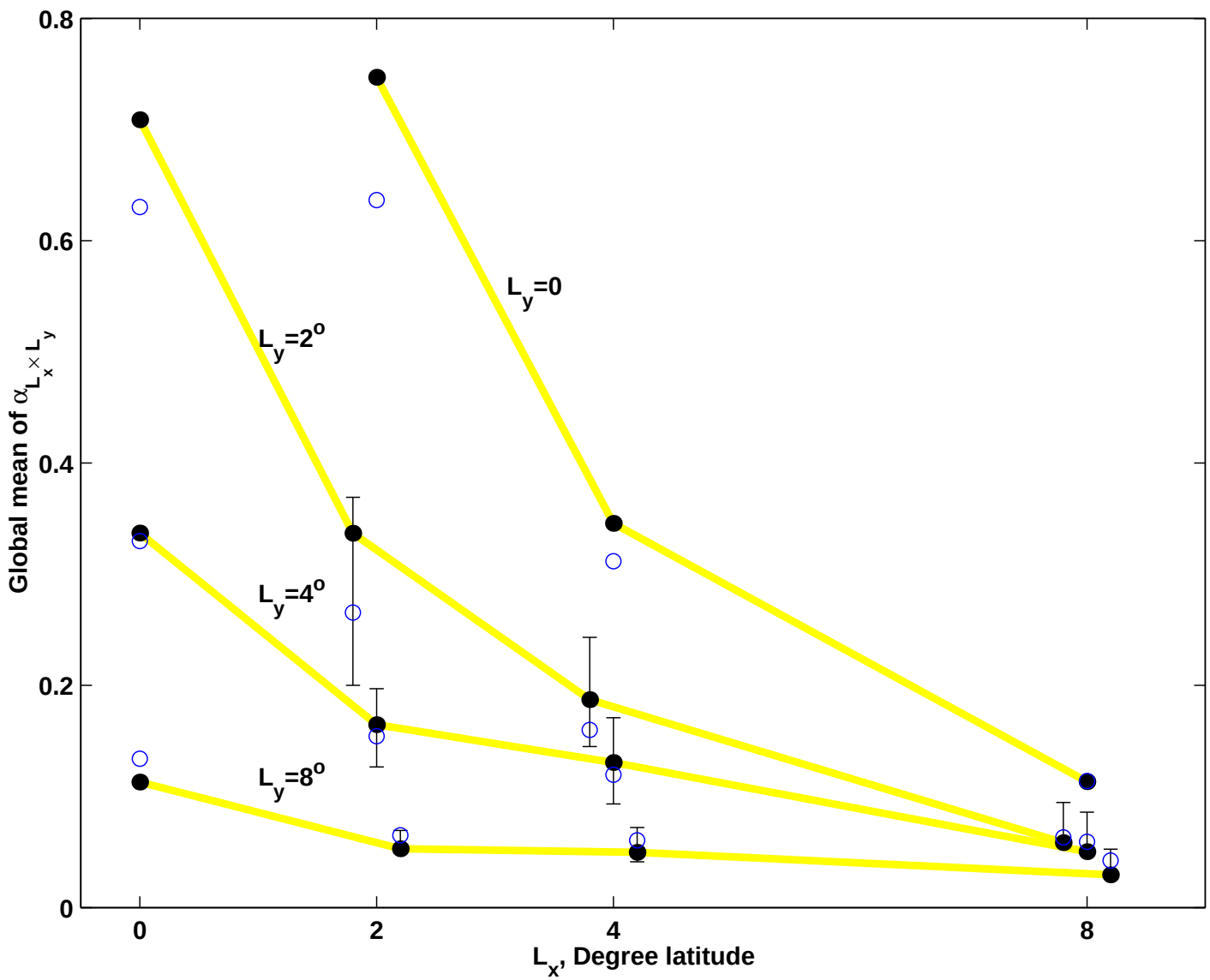

Figure 4. Global means of $\alpha_{L_x \times L_y}$ for L_x and L_y taking values of 2^o, 4^o, and 8^o. Shown are observed values computed from the DLTR data set (empty circles) and theoretical estimates (solid circles) with error bars computed by formula (20). Cases of one dimensional average (L_x or L_y equals to 0) are shown as well.